Direct conversion of glucose to 5-hydroxymethylfurfural over niobium oxide/phosphate-carbon composites derived from hydrothermal carbonization of cyclodextrins

Walid Hamza Saadaoui, Cécile Machut, Sébastien Rio, Sandra Bigot, Vincent Wiatz, Eric Monflier, Anne Ponchel

Direct conversion of glucose to 5-hydroxymethylfurfural over niobium oxide/phosphate-carbon composites derived from hydrothermal carbonization of cyclodextrins

Walid Hamza Saadaoui [a], Cécile Machut [a], Sébastien Rio [a], Sandra Bigot [b], Vincent Wiatz [b], Eric Monflier [a], A. Ponchel [a,*]

[a.] Univ. Artois, CNRS, Centrale Lille, Univ. Lille, UMR 8181, Unité de Catalyse et Chimie du Solide (UCCS), F-62300 Lens, France

[b.] Roquette Frères, 1 rue de la Haute Loge, 62136 Lestrem, France

Corresponding author: anne.ponchel@univ-artois.fr

Keywords: Niobium oxide; Carbon-metal oxides; Cyclodextrins; HMF; Acid catalysis.

Abstract

Direct conversion of glucose to 5-hydroxymethylfurfural was studied in a biphasic system, with phosphated niobium oxide-carbon catalysts. We developed a facile approach to generate Nb-based composites with high metal loadings (~ 20 %) through hydrothermal carbonization (HTC), followed by calcination and H_3PO_4 adsorption. Attention has been paid to the nature of oligosaccharide and amount of water used upon HTC. Catalysts were characterized by XRD, N_2 adsorption, NH_3-TPD, SEM-EDS and XPS. NbP@C-RB30 and NbP@C-RB15 prepared from randomly methylated β-CD in low volumes were found to be more efficient for HMF production, with yields of 32-34 % attained after 3 h in biphasic NaCl-water/methyl isobutyl ketone media. Notably, HTC route provided appropriate conditions for forming acidic Nb_2O_5 nanoparticles, dispersed and maintained over carbon microspheres, and enriched with surface P–OH. These features played an important role for an adequate distribution of the catalyst in the reaction medium composed of two immiscible solvents.

1. Introduction

For decades, utilization of lignocellulosic biomass has become a major research topic, envisioned as an alternative for the production of renewable biofuels, chemicals and polymers to fossil resources [1,2]. In this context, 5-hydroxymethyl-2-furfural (HMF), with the presence of reactive functional hydroxymethyl and aldehyde groups has been identified as a strategic key intermediate between biomass and biochemicals, which can be converted into a variety of other valuable chemicals, including 2,5-dimethylfuran (DMF), levulinic acid (LA), γ-valerolactone (GVL) or also 2,5-furandicarboxylic acid (FDCA) [3-5]. However, one of the major concerns for the cost-effective production of the chemicals mentioned above is the issue of access to selective HMF from sustainable biomass conversion. Indeed, the production costs of HMF are still high, hampered by the occurrence of side reactions in the aqueous phase and by the steps of isolation and separation of HMF [6]. To overcome these limitations, aqueous biphasic systems, in which the HMF can be extracted from the aqueous phase into an organic phase, allow to reduce its residence time in the aqueous reaction medium and improve its protection against further degradation [7]. Many different C3-C6 solvents including alcohols, ketones and ethers, applied alone or in mixture, have been investigated as extracting solvents [8]. A particular attention has been given to methyl isobutyl ketone (MIBK) due to its good partition coefficient, low boiling point, high biodegradability and cheap nature [9]. It is worth mentioning that increases in extraction recovery are achieved by adding chloride salts in the MIBK-water system, such as NaCl through a salting-out effect [10].

The HMF synthesis from the direct conversion of glucose to HMF is an option of choice, because glucose (the main constituent of cellulose) is abundantly and economically accessible in regard to the high diversity of cellulosic biomass feedstocks in nature, with almost no geographical limitations [11]. From a mechanistic point of view, the conversion of glucose to

HMF is assumed to occur following a cascade process, proceeding by the initial isomerization of glucose to fructose promoted by a Lewis acid, followed by the dehydration of the intermediate fructose to HMF by a Brönsted acid. The use of bifunctional catalytic systems with a balanced amount of Lewis and Brönsted acid sites aims at limiting the side-reactions that typically occur with HMF (i.e., the rehydration to levulinic and formic acids or/and polymerization to humins), which lead to poor reaction mass balances. Many different classes of acidic catalysts have been proposed, such as homogeneous (e.g., mineral acids, organic acids and metal salts Lewis acids) and heterogeneous (e.g. acid resins, heteropolyacids, zeolites, sulfated metal oxides, metal phosphates, sulfonated carbons) in aqueous, organic-water [8,12] or ionic liquid media [13]. The use of solid acid catalysts appears advantageous for the simplification of the technological processes by facilitating their isolation from the post-reaction mixture and reuse or recycling.

Among heterogeneous catalysts, niobic acid or hydrated niobium oxide ($Nb_2O_5 \cdot n\ H_2O$), which is known to possess both Lewis and Bronsted acid sites [14], has received a substantially increasing interest for water-related reactions because of the fact that the Lewis acid sites are still active, despite water coordination [15]. Indeed, the catalytic performance of niobic acid in water primarily emerge from the preservation of a particular Lewis acid property in NbO_4-H_2O adducts, with the presence of residual positive on the unsaturated Nb cation [16]. In line with this, niobic acid has been demonstrated to be an effective catalyst for a number of acid-catalyzed reactions involving the release of water molecules, such as the dehydration of glucose to HMF [16,17-19]. The use of phosphoric acid-treated niobic acid or niobium phosphate has also been reported to promote several acid-catalyzed dehydration reactions of carbohydrates, by allowing to increase the number of surface acid sites (as compared to the pure Nb oxide) while maintaining the water-tolerance properties of the acid sites in polar and protic solvents [20-24].

The HMF product can be obtained from the direct conversion of glucose in variable yields between 20 % [19] and 42 % [25] depending on the reaction conditions, but in the vast majority of cases, HMF yields ranging from 30 and 36 % are observed [18, 23,26,27]. Recently, niobium phosphate catalyst has also been implemented in a biphasic continuous flow tubular reactor, affording a yield of 45 % at 150°C under quasi-steady state conditions maintained for 8 h. However, a catalyst deactivation has been observed after 24 h time on stream [24]. The niobium phases can be also dispersed or incorporated in supports, in order to maximize the number of exposed active sites. Thus, silicas [28], zeolites [29], magnetic nanoparticles [30] and carbons [31-33] have been examined as supports for Nb catalysts for the production of HMF from glucose. The supported approach is also an interesting way to improve the hydrothermal stability of catalysts in water at elevated temperatures and pressures [34]. For instance, it has been reported that niobia catalysts supported on a mesoporous silica (SBA-15) exhibited remarkable hydrothermal stability, capable of both preserving the structural organization of SBA-15 and preventing the undesired phase transformation of niobia from an amorphous to a crystalline phase, which is less catalytically active [35]. Among various carriers, carbon materials are known to exhibit excellent hydrothermal stability in the aqueous-phase reaction systems, even in supercritical conditions, thus offering a substantial advantage for biomass conversion applications [36]. In addition, carbon materials are considered as one of the most attractive candidates to produce carbon-based acid catalysts, due to their simple and cost-effective synthesis procedures, availability of carbon precursors (i.e., carbohydrates, sugars, or lignocellulosic biomass), intrinsic chemical functionalities and tunable surface properties. Xiong et *al*. [31] reported that the localization of the carbon-based catalysts in the biphasic environment can be controlled by the preparation conditions and influence the catalytic performance in the dehydration of glucose reaction. Thus, these authors synthesized a series of niobia-carbon composites by deposition-precipitation with different degrees of hydrophilicity,

such as by varying the pretreatment temperature of the carbon black support with nitric acid (80-120°C). It was proposed that the superior activity of the Nb/C catalyst prepared from using the more hydrophilic carbon black support (pretreated in HNO_3 at 120°C) reflects its stronger affinity for the water phase, rather than any significant acid effect (even though surface acid properties were not determined in this work). Poorer activities were obtained when the Nb/C catalyst was positioned in the organic phase (pretreated at 80°C) or in the interfacial region (deposition-precipitation-carbonization) due to a lack of contact with the hydrophilic glucose molecules. Using a one-pot hydrothermal carbonization method with niobium tartrate and glucose as precursors in the presence of p-toluene sulfonic acid and citric acid, Li et al. also demonstrated that, with an optimized catalyst formulation (~ 50 wt. % Nb_2O_5), good yields of HMF could be achieved from the conversion of glucose (59 %) after 8 h of reaction at 170°C in a THF/H_2O biphasic system. The catalyst scope was successfully extended to the synthesis of HMF from cellulose. These encouraging results were attributed to the bifunctional nature of the catalyst, with the concurrent presence of Lewis and Brönsted acid sites of weak to medium strength [32].

With these data in our hands, it occurred to us that cyclodextrins could be used as suitable precursors for the preparation of niobia-carbon composites by hydrothermal carbonization. Cyclodextrins (CDs) are water-soluble cyclic oligosaccharides, which are industrially produced by the enzymatic degradation of starch and composed of *n* glucopyranose units (*n* = 6 for α-CD, 7 for β-CD and 8 for γ-CD). Since the mid-1990s, CDs are commercially produced in large quantities at reasonable prices, such as US $ 3-4 /kg for β-CD for industrial applications [37,38]. These molecules have a truncated cone structure, with a hydrophobic interior and a hydrophilic exterior due to the presence of abundant available hydroxyl groups. CDs appear to have multifunctional properties, such as the formation of inclusion complexes, stabilization of metal

NPs and coordination of metal ions, induced by molecular recognition or attractive electrostatic interactions with the hydroxyl groups [39,40]. Random modifications of primary and secondary hydroxyl groups can also be realized with a variety of substituents, *e.g.* alkyl, hydroxyalkyl, carboxyalkyl, amino, *etc.,* to modulate properties, such as complexation ability and solubility in water. Indeed, the presence of these substituents disrupts the hydrogen bonding network that naturally exists in native CD molecules, which increases the ability to interact with surrounding water solvent molecules, with sometimes an increase of more than a factor of 100 in the aqueous solubility [41]. Although the potential of cyclodextrins has been the subject of several investigations for the synthesis of pure carbon nanostructures [42-48], the number of reports on the synthesis and properties of metal-carbon composites is still limited, especially by hydrothermal carbonization. Indeed, most of the work has focused on pyrolysis methods with mixtures of cyclodextrins and metal precursors (assisted or not by additional organic [49] or inorganic [50] structure-directing agents) and on templating techniques using inorganic sacrificial materials [51,52]. Yet, hydrothermal carbonization (HTC) of high carbon-content materials (i.e. sugars, starch, cellulose, lignocellulosic biomass or wastes) have gained interest for its potential to produce tailored carbon materials for diverse applications such as energy storage and conversion and heterogeneous catalysis [53]. Several advantages can be derived from the HTC method, such as the ease of operation, low cost and process energy efficiency. Indeed, the carbonization treatment occurs in aqueous solution under relatively mild temperature conditions (typically in the range between 160°C and 250 °C) and pressure conditions (autogenous), without the need to pre-dry the carbon feedstock.

In the present study, we attempt a detailed study of the effect of cyclodextrins in the preparation of phosphated niobium-carbon composites by HTC, using ammonium niobium oxalate as the metal precursor. More precisely, we have focused our attention on different CDs, native CDs

(α-CD, β-CD and γ-CD) and randomly modified CDs, such as hydroxypropylated β-CD and methylated β-CD, the latter two family being available with various degrees of substitution on an industrial scale [41]. The applied synthesis methodology can be summarized in three main steps: *i)* HTC of the precursor solution (cyclodextrin, urea and Nb salt) at 200 °C for 24 h, *ii)* Pyrolysis at 400 °C under a N_2 atmosphere and *iii)* Post-treatment with phosphoric acid. Step *ii)* and step *iii)* were performed respectively to increase the homogeneity of the composite CD-derived composite hydrochar in terms of composition and texture (thermal activation) [54] and to introduce phosphate groups for preventing the crystallization of less active Nb_2O_5 particles [55]. Our idea was to take advantage of CDs to act as carbon sources and as chelating agent for the metallic cations in order to facilitate the generation of homogeneous and finely dispersed oxide phase in contact with the carbon surfaces. In this context, we especially investigate the influence of the chemical nature of the cyclodextrins used, native or chemically modified, and their concentrations during the HTC process. The substitution pattern of modified β-CD by 2-hydroxypropoxyl groups (HP-β-CD) or methyl groups (CH_3) are known to affect the physicochemical properties of the cyclodextrins, causing changes in the solubility and surface activity behaviors in aqueous media, especially with high degrees of substitution [56]. This may have consequences on their reactivities and transformation mechanisms occurring upon HTC conditions, especially those involving the hydrolysis of the oligosaccharides. The as-obtained NbP@C catalysts are investigated in the direct conversion of glucose to HMF and the structure-activity relationship is discussed on the basis of a number of physicochemical characterizations.

2. Experimental section

2.1. Chemicals

α-cyclodextrin (α-CD), γ-cyclodextrin (γ-CD) and randomly methylated β-cyclodextrin (RaMe-β-CD, MW = 1311 $g.mol^{-1}$, average DS = 12.6) were purchased from Wacker Chemie.

CRYSMEB®, which was a gift from Roquette Frères (Lestrem, France), is a low methylated β-CD product, with isomers mainly substituted on the secondary side (MW = 1191 g.mol^{-1}, average DS = 4). 2-hydroxypropyl-β-cyclodextrin (HP-β-CD, MW = 1460 g.mol^{-1}, average DS = 5.6) was also supplied as a gift by Roquette Frères (Lestrem, France). The chemical structure of cyclodextrins used in this study is gathered in Table S1. Ammonium niobate(V) oxalate hydrate ($C_4H_4NNbO_9 \cdot xH_2O$) and D-(+)-Glucose ($C_6H_{12}O_6$) were purchased from Sigma-Aldrich, 5-hydroxymethylfurfural (98 % purity) from Acros Organics, and ultra-purified HPLC water from Honeywell company (USA). All other reactants and solvents were obtained from Fisher Scientific in their highest purity and were used without any further purification or drying.

2.2. Catalyst preparation

The phosphated niobia-carbon materials were prepared by hydrothermal carbonization, using a protocol adapted from Xiong et al. [31]. The quantities of reagents were calculated in order to produce composite materials, with a nominal loading of about 20 wt. % of niobium. The main steps of the catalyst preparation are schematically represented in Scheme 1. In a typical synthesis, 6.2 g of cyclodextrins were dissolved in a specific volume of deionized water (15 - 150 mL) to which were successively added 3.4 g of ammonium niobium oxalate and 1.02 g of urea. The mixture was placed in a Teflon lined hydrothermal synthesis autoclave reactor and was subjected to heating at 200 °C for 16 h. The resulting brown-to-black solid product was recovered by centrifugation and washed by sequential washing-centrifugation-supernatant removal (4 cycles) with deionized water. After drying overnight at 100°C and grinding to powder, the solid sample was carbonized at 400°C for 4 h in a nitrogen flow (50 mL min^{-1}). Then, the niobia-carbon material (1g) was immersed in 200 mL of an aqueous solution of H_3PO_4 (1 M). After 48 h under stirring at room temperature, the dispersion was filtered and the collected solid was thoroughly washed with deionized water until phosphate ions were no

longer detected. Finally, the solid was dried overnight at 100°C. The as-prepared materials are designated as NbP@C-CD*x*, where CD represents the nature of the cyclodextrin used (with α-CD and γ-CD for the native cyclodextrins and, with RB, CR and HP for the RaMe-β-CD, CrysMe-β-CD and HP-β-CD, respectively) while *x* indicates the water volume used to dissolve the cyclodextrin. As an example, NbP@C-RB60 corresponds to a phosphated niobia-carbon composite prepared with RaMe-β-CD as the carbon source in a volume of water of 60 mL.

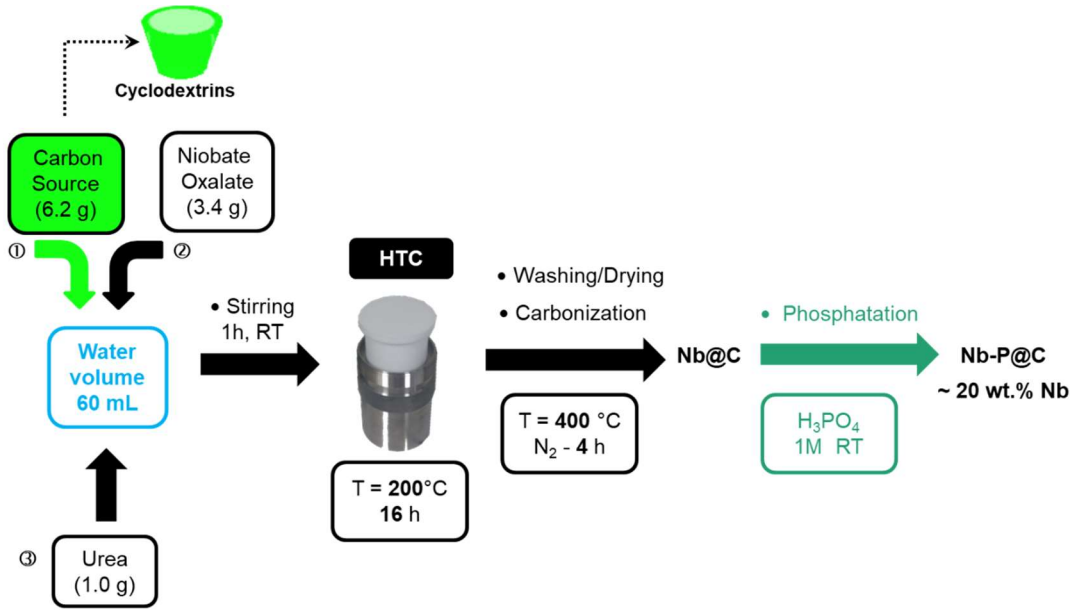

Scheme 1. Schematic illustration of the synthesis of NbP@C-CD60 materials by hydrothermal carbonization using cyclodextrins as carbon sources

2.3. Physicochemical characterizations

Metal loadings from elemental analysis. Elemental analyses of the composite samples (niobium and phosphorous) were performed by inductively-coupled plasma optical emission spectroscopy (iCAP 7000 Thermo Scientific ICP-OES) after a digestion step. Microwave acid digestion was carried out as follows: 10 mg of NbP@C sample was weighed and transferred into a pressure-resistant PTFE vessel and 20 mL of concentrated H_2SO_4 (96 wt. %) was added to the sample. The vessel was closed and heated to 230°C for 1 h in the microwave oven (CEM Mars instrument, Power 600 W). The resulting solution was finally diluted with pure water up

to a final volume of 100 mL. The contents of niobium and phosphorous initially present in the solid composite were estimated by ICP-OES using an external calibration with Nb and P standard solutions.

Acid titration measurements. The total acidity of the phosphated niobia-carbon composites was determined by Boehm's titration method [57]. In a typical experiment, 50 mg of NbP@C sample was equilibrated for 24 h with 20 mL of NaOH (0.1 mol L^{-1}). Then, 5 mL of the filtrate was back-titrated with HCl (0.1 mol L^{-1}) using an automatic titrator (Hach Titralab AT1000). The numbers of acidic sites were calculated from the assumption that NaOH could neutralize all acidic oxygen groups, including carboxylic, lactonic and phenolic groups. Each Boehm's titration result corresponds to an average of at least two measurements.

Powder X-ray diffraction (wide angle). Wide angle XRD patterns were collected at room temperature on a Bruker D8 Advance diffractometer in Bragg Brentano geometry equipped with a copper anode (λ= 1.5418 Å for Cu Kα) and a 1D PSD Lynxeye detector. The scattering intensities were measured over an angular range of $5° < 2\theta < 80°$ with a step-size of 0.02° and a counting time of 2 s per step.

Porosity measurements. Nitrogen adsorption-desorption measurements were performed at -196°C on a Micromeritics Tristar 3020 system. The resulting data were analyzed using the Tristar II 3020V1.03 software. The specific surface areas for nitrogen adsorption were calculated using the Brunauer-Emmet-Teller (BET) model in the relative pressure (P/P°) range of 0.05-0.25 while the pore size distributions were obtained from the adsorption branch using the Barrett-Joyner-Halenda (BJH) method. The total pore volumes were estimated at P/P° = 0.995 assuming that all the pores were completely filled with liquid nitrogen. Prior to adsorption analysis, each sample was outgassed at 250°C for 3 h under vacuum.

Scanning Electron Microscopy (SEM). Before SEM examination, the powdered catalysts were dispersed in ethanol, sonicated for 5 min. Then a drop of the dispersion was deposited onto the

alumina holder and left until complete evaporation. SEM observation was operated on a Hitachi SU3800 equipped with a tungsten hairpin filament. Imaging was performed at different acceleration voltages (3, 7 and 15 kV). Energy dispersive X-ray spectroscopy (EDS) was also performed as a complement to the SEM observation operating at an acceleration voltage of 7 kV and working distance of 10 mm by using a Bruker Xflash 6/30 (Quantax Esprit) detector.

X-ray Photoelectron Spectroscopy (XPS). The surface composition of the composites was analyzed by XPS using a Kratos Axis Ultra DLD apparatus equipped with a hemispherical analyzer and a delay line detector. The spectra were recorded using an Al monochromated X-ray source (10 kV, 15 mA) with a pass energy of 40 eV (0.1 eV/step) for high resolution spectra, and a pass energy of 160 eV (1 eV/step) for survey spectrum in hybrid mode and slot lens mode, respectively. The C1s binding energy (284.7 eV) was used as an internal reference. Peak fitting and deconvolution of the experimental photopeaks was performed by CasaXPS software. Prior to the analyses, the solid samples were subjected in the pre-treatment chamber to a heating at 120°C for 1 h under air flow (50 mL (STP) min) to eliminate traces of a water or impurities adsorbed.

Temperature Programmed Desorption of NH_3 (TPD-NH_3). The acidity of the NbP@C composites was evaluated by temperature-programmed desorption of ammonia (NH_3-TPD) using a chemisorption analyzer (AutoChem II 2920, Micromeritics). Prior to adsorption, approximately 100 mg of catalyst, placed in a reaction tube, was pretreated in helium atmosphere at 250°C for 0.5 h in order to remove any water or adsorbed volatile contaminants. The sample was further cooled to 100°C, and a mixture of NH_3 (10 % in He) was injected at a flow rate of 40 mL min^{-1} to saturate the surface with NH_3. Then, the physically adsorbed probe molecule was eliminated by flowing He gas for (40 mL.min^{-1}) for 2 h at 100°C. Then, the furnace temperature was increased from 100 to 600 °C at a heating rate of 10 °C min^{-1} under helium to desorb chemisorbed NH_3. The exhaust gas was analyzed by an on-line thermal

conductivity detector (TCD) and by a Pfeiffer quadrupole mass spectrometer connected with the outlet chemisorption analyzer. The mass spectrometer followed the NH_3 desorption by m/z = 15.

2.4. Catalytic tests and analysis

The catalytic experiments were performed in a two-phase reaction system consisting of water/MIBK (vol:vol 1:3), in batch conditions, using a 25 mL mechanically stirred autoclave reactor (Hastelloy, Parr Instrument). In a typical experiment, 200 mg of catalyst, 3 mL of an aqueous solution of glucose (3.33 wt. %) and 9 mL of MIBK were introduced into the reactor. NaCl (1 g) was also added to the reaction medium for improving the efficiency of the HMF extraction capacity of the organic phase. After closing, the autoclave reactor was pressurized to 20 bar of argon and heated up to 150 °C. When it was raised to the desired temperature, the mixture was stirred at 1400 rpm and zero time was taken. After reaction for a given period of time (typically 3 h), the reaction was quenched in an ice-cold water bath and the reaction mixture was carefully collected by rinsing the reactor several times with water (12 mL). Then, the resulting aqueous and organic phases were separated by centrifugation and analyzed separately and independently with a high-performance-liquid-chromatography (HPLC Shimadzu Nexera 30) equipped with two different detectors: an evaporative light scattering detector and a photodiode array detector. The HPLC apparatus was equipped with a Rezex RCM column (300 × 7.8 mm, Phenomenex) and used at 80°C with HPLC deionized water at a flow rate of 0.6 mL min^{-1} as the mobile phase. The amounts of each individual compound (Glucose, Fructose and HMF) were determined using specific calibration curves obtained by analyzing synthetic standard solutions with known concentrations. Each catalytic run was performed in duplicate at least, and the reported results are the average between the two runs with an experimental error of ±2.5%. The data given for the quantification for HMF refer to the sum of the contributions deriving from the aqueous and organic phase. The conversion of

glucose, selectivity and yield for fructose and HMF, and the mass balance are calculated according to equations 1-4 below:

- $\text{Conversion (\%)} = \frac{\text{mol}_{\,initial\ glucose} - \text{mol}_{\,final\ glucose}}{\text{mol}_{\,initial\ glucose}} \times 100$ (1)

- $\text{Selectivity}_i\ (\%) = \frac{\text{mol}_{\,i\ produced\ (aqueous\ phase\ +\ organic\ phase)}}{\text{mol}_{\,initial\ glucose} - \text{mol}_{\,final\ glucose}} \times 100$ (2)

- $\text{Yield}_i\ (\%) = \frac{\text{mol}_{\,i\ produced\ (aqueous\ phase\ +\ organic\ phase)}}{\text{mol}_{\,initial\ glucose}} \times 100$ (3)

- $\text{Mass balance (\%)} = \frac{\text{mol}_{\,final\ glucose} + \sum_i \text{mol}_{\,i\ produced\ (aqueous\ phase\ +\ organic\ phase)}}{\text{mol}_{\,initial\ glucose}} \times 100$ (4)

3. Results

3.1. Catalyst screening: effect of cyclodextrin as carbon source

In a first screening, we have decided to examine the effect of the nature of CDs as potential carbon sources in the preparation by HTC of NbP@C catalysts for the direct conversion of glucose to HMF. This study, which aims at quickly identifying the most relevant CDs to be used during the HTC process, focuses on five CDs, native (α-CD and γ-CD) and chemically modified (RaMe-β-CD, CRYSMEB® and HP-β-CD). All other synthesis parameters are kept constant (in particular, the volume of water used for HTC was fixed at 60 mL and the weight amount of the oligosaccharide at 6.2 g). Note that, under these concentration conditions, the use of β-CD had to be ruled out due to its too low solubility in water (1.85 g per 100 mL at 25°C).

Table S2 shows the main characterization results obtained for the different NbP@C-CD60 samples, in terms of elemental analysis, acidity and N_2-adsorption. The niobium and phosphorous contents present in each material have been determined by ICP-OES analysis. The niobium content falls in the range 21.6-26.0 wt.%, with an average value of 23.7 ± 1.9 wt. %.

Regarding the ICP-OES analysis on phosphorous, the results also show that the phosphoric acid treatment method used allow a fairly homogeneous P-loading, whose average content is 1.3 ± 0.2 wt. %. In terms of structural properties, the X-ray diffraction patterns of the NbP@C-CD60 samples appear very similar, being consistent with a fairly low degree of crystallization regardless of the carbon source used (Figure S1). Indeed, the XRD plots indicate a mixture of pseudohexagonal TT-Nb_2O_5 phase (JCPDS: 00-028-0317), coexisting with poorly crystallized or amorphous Nb_2O_5 [58]. As the acidic properties play an important role in the mechanisms of glucose dehydration, the contents of acidic oxygen surface functional groups have also been estimated by Boehm's titration (Table S2). It is found that the total acidity is only slightly affected by the nature of the cyclic molecule used, varying between 3.28 and 3.67 mmol g^{-1}. This is indicative of a surface rich in acid groups including carboxylic acid, lactonic, and phenolic groups. NbP@C-CD60 materials featured also similar textural properties: specific surface areas close to 85 m^2/g, pore volumes of 0.3-0.4 cm^3/g and pore diameters of *ca*. 15 nm.

The catalytic performance of the NbP@C-CD60 materials has been evaluated in the catalytic transformation of glucose to HMF at 150°C, and the results after 3 h of reaction are given in Figure 1. It can be noted that, among this series of samples, the catalytic performance is not greatly influenced by the nature of the cyclodextrin used during the HTC synthesis process. We observe that the NbP@C-CD60 catalysts prepared from native CD and chemically modified CDs exhibit similar conversions in the range of 58-63% and HMF yields in the range 19-27 % after 3 h of reaction. This behavior reflects the overall similar compositions and structures, in line with what has been described above. At this reaction time, the mass balance of the reaction reaches between 67 and 77 %, indicating that some side-reactions, including rehydration of HMF and cross-polymerization to form humins take also place. However, note that, upon using RaMe-β-CD, a slight but perceptible improvement in catalytic performance seems to be

observed for NbP@C-RB60, which offers the best balance between conversion (64 %), HMF selectivity (42%) and yield (27 %). It is also worth mentioning that the repeatability of the synthesis protocol has been validated by testing another sample from a second synthesis batch (see NbP@C-RB60 no.2 in Figure 1).

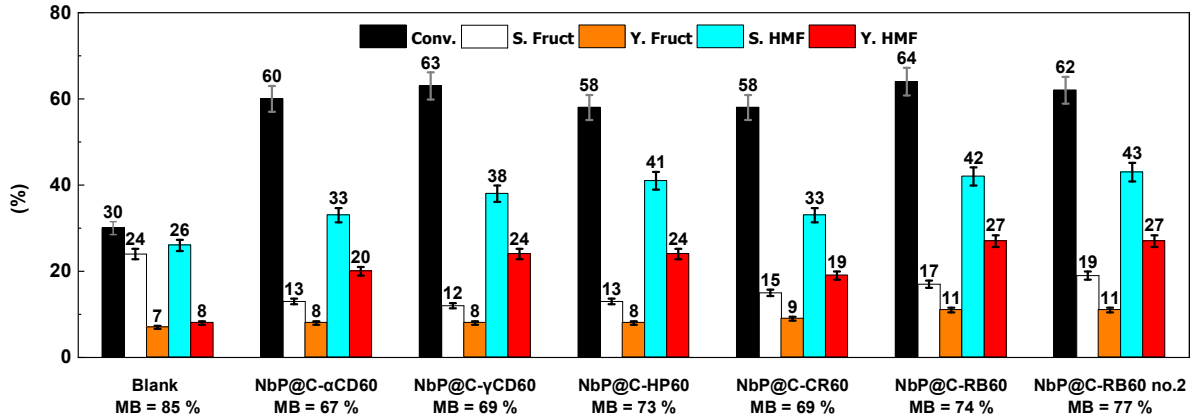

Figure 1. Aqueous phase conversion of glucose over NbP@C-CD60 materials prepared with various cyclodextrins, and corresponding selectivity, yield for fructose and HMF and mass balance. The value in percentage of mass balance (MB) is indicated below the name of the sample. NbP@C-RB60 no.2 corresponds to results for a second synthesis batch. *Reaction conditions*: *Glucose concentration (3.33 wt. %); Catalysts mass: 0.2 g; Solvent: 3 mL H_2O (NaCl 33 %) and 9 mL MIBK (as extracting solvent); Reaction temperature: 150°C; Reaction time: 3 h. . Pressure: 20 bar Ar.*

The precision of the catalytic measurement was further assessed by repeating three times, each in duplicate, the catalytic experiment under the same conditions (150°C, 3 h, aqueous biphasic conditions) on NbP@C-RB60 (Table 1). NbP@C-RB60 gives almost identical results, in terms of activity and selectivity (Entries 1-3). Further confirmation of the stability of the formulation was demonstrated by performing a recyclability test, as briefly described above. After the first run (3h), the catalyst is recovered by centrifugation, washed by three sequential washing steps with deionized water (200 mL per washing cycle) and dried at 100°C for 24 h before to be reused in the following catalytic run. As shown (Entry 4), the catalyst remains efficient in its

reuse cycle, with a glucose conversion and HMF yield of 63 % and 25 %, respectively, corresponding to percent differences of only 2 % and 7 %. Note that this recycling behavior is satisfactory when compared to the literature, this catalyst being more resistant to deactivation as compared to some previously studied systems, such as for instance Al-MCM-41 [59], Sn-MCM-41 [60], SO_3H-OAC [61], NbP [24] or also GHNb1.2 obtained by deposition-precipitation [30]. Additionally, there is no evidence of the deterioration of this catalyst, as shown by BET and XRD (Figure S2). The origin of this stability can be analyzed by the preparation method of NbP@C catalysts through the synthetic HTC process, with the presence of the niobium salt and urea, in addition to the cyclodextrin. This method would promote high level of niobium incorporation and strong interaction with the carbon matrix [32].

Table 1. Reusability test of the NbP@C-RB60

Entry	Glucose conversion (%)	Frutose selectivity (%)	Fructose yield (%)	HMF selectivity (%)	HMF yield (%)	Mass Balance (%)
1[a]	64	17	11	42	27	74
2[a]	65	17	11	41	26	71
3[a]	64	15	11	43	28	73
4[b]	63	18	11	40	25	74

Reaction conditions: Catalyst: NbP@C-RB60; Glucose concentration: 3.33 wt. %; Solvent: 3 mL H_2O (NaCl 33 %) and 9 mL MIBK (as extracting solvent); Reaction temperature: 150°C; Reaction time: 3 h. [a.] Results after the first run performed on the same batch of fresh catalyst; [b] Results after the second run performed on the spent catalyst (solid catalytic mixture recovered after run 1).

3.2. Effect of the volume of water: physicochemical characterization

With these results in hands, we have decided to continue this study by giving priority to RaMe-β-CD as cyclodextrin. Indeed, its high solubility and interfacial or surface tension effects could play a role in the self-assembly of the colloidal composite particles during the HTC process at meso- and macroscale levels and influence the structuration and consequently catalytic

performance of the resulting NbP/C catalysts. In line with this, the RaMe-β-CD concentration in the synthesis mixture was evaluated as another synthesis parameter of the phosphated niobium-carbon composites by HTC. Indeed, the presence of a large number of methyl groups on the CD rims (DS = 12.6) is a well-known factor affecting the physicochemical properties of the cyclodextrins, both in terms of water solubility (through the disruption of intermolecular hydrogen bonds) and surface-activity (through to the presence of hydrophilic and hydrophobic microenvironments) [56]. In contrast, the native CDs and chemically modified CDs with low degrees of substitution are known to show no or only negligible surface activity [62]. Thus, the surface tension curve of RaMe-β-CD upon increasing its concentration reveals the decrease in surface tension values, with a more pronounced drop in the higher concentration region, typically beyond 80 mM (concentration used for the preparation of NbP@C-RB60) (Figure S3). This observation suggests that the surface-active characteristics of RaMe-β-CD could induce significant changes in the pre-organization of the starting reagents that occur in solution, and could reduce the surface energy of the solid particles during coarsening in the solid-liquid suspension systems. In line with this, we have decided to examine the effect of the concentration parameter by varying the volume of water used to solubilize the starting reagents (V = 15, 30, 60, 90, 120 and 150 mL) while keeping the mass of RaMe-β-CD constant (m = 6.2 g). In the following, the physicochemical characterization and catalytic performance of these NbP@C-RB*x* materials towards the direct glucose conversion to HMF will be subsequently examined.

3.2.1. Structural properties of catalysts

Elemental analysis of this series of catalysts prepared with various volumes of water confirms satisfactory loadings of phosphorous (~ 1-2 wt.%) and niobium (~ 22-23 wt.%) (Table 2). The resulting catalysts have been further characterized by X-ray diffraction (Figure 2). No obvious difference can be distinguished from the XRD patterns. According to what was previously

observed, the XRD profiles reveal that, for this series of samples of varying water contents, both pseudohexagonal TT-Nb_2O_5 and amorphous niobic acid Nb_2O_5 are again obtained, with no apparent change in their relative proportion. The persistence of the amorphous Nb_2O_5 phase is evidenced by the presence of broad and weakly intense bands at around 2θ = 25° and 55°, irrespective of the volume of hydrothermal synthesis [58].

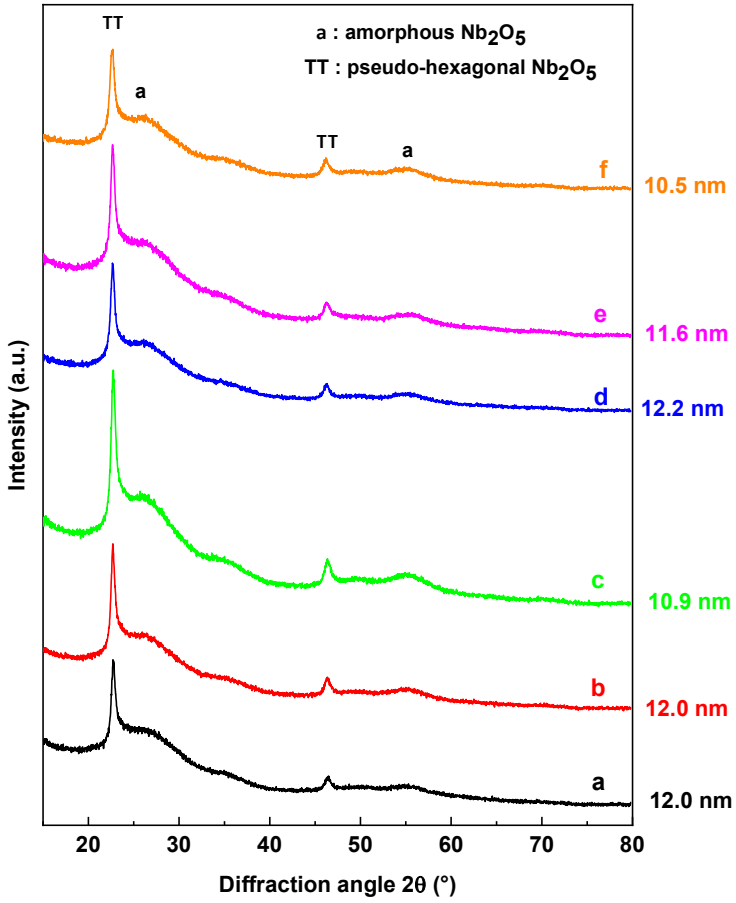

Figure 2. XRD patterns of NbP@C-RB*x* catalysts prepared by HTC from RaMeβ-CD in different volumes of water: (a) NbP@C-RB15, (b) NbP@C-RB30, (c) NbP@C-RB60, (d) NbP@C-RB90, (e) NbP@C-RB120 and (f) NbP@C-RB150. The numbers in the right side indicate the average crystallite size of Nb_2O_5 (200) estimated from the Scherrer equation.

3.2.2. Textural properties of catalysts

Textural properties of NbP@C-RB*x* materials, including BET specific surface area, total pore volume and pore size are also gathered in Table 2. For the lower range of RaMe-β-CD

concentration between 30 mM (V = 150 mL) and 50 mM (V = 90 mL), similar N_2 adsorption isotherms (type IV) are observed, exhibiting hysteresis loops at high relative pressure range of about 0.8-1 (Figure S4). Such H3 type pores are consistent with interparticle porosity and non-uniform pores. Although the specific surface area is little affected in this range of volume, the pore-size distribution appears to be altered and shifted to larger pores (from 12.9 to 19.6 nm). When the hydrothermal volume is fixed at an intermediate value of 60 mL, it is seen that the sample has the highest specific surface area (121 m^2/g). Conversely, decreasing the volume of water from 60 mL to 15 mL follows an opposite trend with respect to the specific surface area and pore volume. Thus, for the composite material prepared with the lowest volume of water, NbP@C-RB15, the specific surface area and pore volume drop sharply to small values (33 m^2/g and 0.048 cm^3/g, respectively). However, the pore-size distribution becomes significantly narrower, with smaller and more uniform mesopores (~ 4.5 nm). This observation is also consistent with the high percentage of mesopores present in this material (98 %). The use of a higher concentration of RaMe-β-CD (315 mM for V = 15 mL), taking part as building units in the HTC process, could lead to a higher density of crosslinking during the formation of solid hydrochar particles, which is favorable to the growth of carbon spheres [63]. It is worth noting that, at this concentration, RaMe-β-CD has a low surface tension value of 47.5 mN/m.

Table 2. Properties of NbP@C-RB*x* materials prepared by HTC from RaMe-β-CD and different volumes (V = 15 to 150 mL) for direct conversion of glucose to HMF

Sample	Nb (wt. %)[a]	P (wt. %)[a]	Total Acidity (mmol/g)[b]	S_{BET} (m^2/g)[c]	Pore volume (cm^3/g)[d]	Pore diameter (nm)[e]	% mesoporosity [f]	r (μmol h^{-1} m^{-2}) [g]
NbP@C-RB15	21.5	1.2	1.51	33	0.048	4.5	98	16.1
NbP@C-RB30	17.8	1.4	2.36	86	0.217	10.2	95	6.78
NbP@C-RB60	23.5	1.2	3.28	121	0.404	14.3	49	3.67
NbP@C-RB90	23.1	2.0	3.71	93	0.287	12.9	47	4.48
NbP@C-RB120	23.2	1.2	3.33	98	0.304	16.4	41	3.91
NbP@C-RB150	22.4	1.0	3.03	95	0.404	19.6	53	4.21

[a] The weight percentage was determined determined by ICP-OES.[b] The total acidity was determined by the Boehm's titration.[c] The specific surface area was calculated from the Brunauer-Emmet-Teller equation in the P/P° range of 0.025-0.20.[d] Total pore volume was estimated at P/P°=0.95. [e] The pore diameter was estimated by the Barrett-Joyner-Halenda method.[f] The mesopore percentage was determined by diviving the mesopore volume by the total pore volume.[g] Rate of HMF formation per unit surface area measured after 1 h of reaction (conversions below 50%) at 150°C in the direct transformation of glucose under biphasic conditions.

3.2.3. Acidic properties of catalysts

Table 2 compiles the data obtained from Boehm's titration on all investigated NbP@C-RB*x* samples. The total number of acidic oxygen surface functional groups is found to vary between 1.51 to 3.71 mmol g^{-1} and this variation correlates quite well with the BET specific surface area of the catalysts. Further insight on the strength of acidity can be gained by temperature programmed desorption of ammonia (NH_3 TPD). Figure 3 plots the NH_3 TPD profiles of a representative selection of NbP@C catalysts prepared from RaMe-β-CD (V = 30, 60 and 90 mL) and their deconvoluted peaks fitted by a Gaussian function.

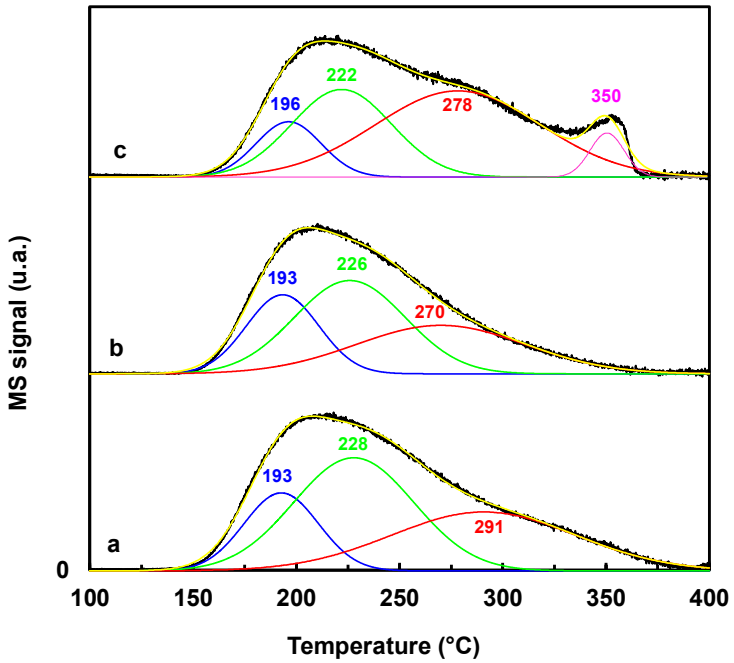

Figure 3. NH_3-TPD of the (a) NbP@C-RB30, (b) NbP@C-RB60 and (c) NbP@C-RB90 materials. The dark-blue and green lines represent the component peaks assigned to weak acid sites (curve maximum below 250°C) while the red and pinks lines are assigned to medium acid sites (curve maximum above 250°C). The yellow lines correspond to the simulated TPD envelopes.

All the NH_3-TPD profiles exhibits a broad distribution of acidity, from 150 to 400°C. It is generally accepted that the NH_3 desorption peaks at the lower temperature range (<250 °C) are assigned to ionic NH_4^+ species, indicative of the protonation of NH_3 on weak Bronsted acid

sites. From 250°C to 500°C, the desorption peaks are assumed to correspond to medium strength acid sites of Brönsted and Lewis type (NH_3 coordinated to the niobium centers), without being able to distinguish between them. Deconvolution of the NH_3-TPD curves of the selected samples exhibits similar components at temperatures lower and higher than 250 °C, confirming the presence of weak Brönsted and medium acid centers on each catalyst surface. The latter acidity can be related to different surface species, such as Nb = O groups and -OH groups arisen from Nb-OH or P-OH or organic acid still present in the composite structures. From the NH_3-TPD profiles and their quantification (Table S3), it can be seen that NbP@C-RB90 contains a number of medium strength acid sites that is higher than those of the other two counterparts. For the materials from RaMe-β-CD prepared in 30 and 60 mL, the ratio of weak acid sites to medium acid sites is in the range 1.8-1.9 while it decreases to about 0.8 for the NbP@C-RB90 material. Besides, one additional NH_3 desorption peak indicating the presence of a new population of medium acid centers is also observed at 350°C (profile c, Figure 3).

3.2.4. XPS analysis of catalysts

XPS analysis has been used to characterize the chemical state and composition of the surface of catalysts. The survey spectra infirm the presence of Nb, P, N, O and C on their surface, as illustrated, for example, for the NbP@C-RB15 material in Figure S5. XPS spectra of the Nb 3d, P 2p, C 1s and O 1s core levels are plotted in Figure 4 (A-D) for NbP@C-RB15 and in Figures S6 to S10 for the remaining samples of the series. Binding energies (BEs) of all the elements and their relative contents are listed in Table 3. Figure 4A shows a well resolved Nb 3d doublet at BEs of 207.1 eV (Nb $3d_{5/2}$) and 210.0 eV (Nb $3d_{3/2}$), which are assigned to Nb(V) species in an oxide environment, and not to niobium phosphate species [64]. There is no apparent difference in the Nb 3d peak position and peak shape between the six samples analyzed. Regarding the surface phosphorous species, the P 2p XPS spectra for the NbP@C-

RB*x* samples are characterized by a single peak with BEs centered at 133.7 - 134.0 eV, these values being typical of pentavalent tetracoordinated phosphorus (PO_4) connected with carbon atoms through C−O−P linkages (phosphate-like structures) [65]. Thus, the XPS spectra of the C1s core level can be deconvoluted into four main components, as shown in Figure 4C, attributable to carbon species in C-C, C=C and C–H (component I, 284.6-284.9 eV), C–OH and C-O-C and/or C-O-P or C-O-N (component II, 285.6–286.0 eV), carbonyl C=O (component III, 287-287.5 eV) and in π-π* transitions in aromatic ring (shake-up satellite peak) (component IV, 290.7-291.3 eV) functionalities. It is worth noting that no evidence of carboxyl HO-C=O groups, which are typically reported at about 289 eV [66] has been found in NbP@C-RB*x*, irrespective of the water volume used during HTC. Interestingly, examination of the O 1s XPS spectra can complement these data obtained from XPS analysis of the C 1s region. The deconvoluted spectra of the O1s core level results in three main components at the following BEs: 529.9-530.2 eV (component I), 531.0-531.2 eV (component II), and 532.9-533.0 eV (component III). The component I can be assigned to surface lattice oxygen (O^{2-}) species in Nb-O oxides, in good agreement with the literature [**Erreur ! Signet non défini.**,67], while the component II can correspond different oxygen surface functionalities, including oxygen double bonded to carbon (C=O) or to phosphorus in the phosphate groups (P=O). The last component at about 533 eV can be attributed to single bonded oxygen in (-O-) in C-O-C, C-O-H or C-O-P surface groups. Notably the surface concentrations measured from the XPS spectra indicate that a higher density of surface Nb species are present in the phosphated niobium-carbon composites when they are prepared using RaMe-β-CD with a volume of water of 30 mL and below (Nb:C = 0.117 for NbP@C-RB15 and Nb:C=0.103 for NbP@C-RB30 against at most 0.063 for the other samples). Even if the differences are less pronounced, a similar trend is also observed for the Nb:O surface molar ratios, showing ratios of 0.268 and 0.255 for NbP@C-RB15 and NbP@C-RB30 respectively. In addition, the relative contribution of the O 1s-I species

corresponding to Nb-O bonding is also higher for the latter two materials, with a maximum relative content of 34 % for NbP@C-RB15. Taken together, these results indicate that a higher dispersion of the niobium oxide phase onto the carbon framework is obtained by using the two highest concentrations of RaMe-β-CD during the HTC process.

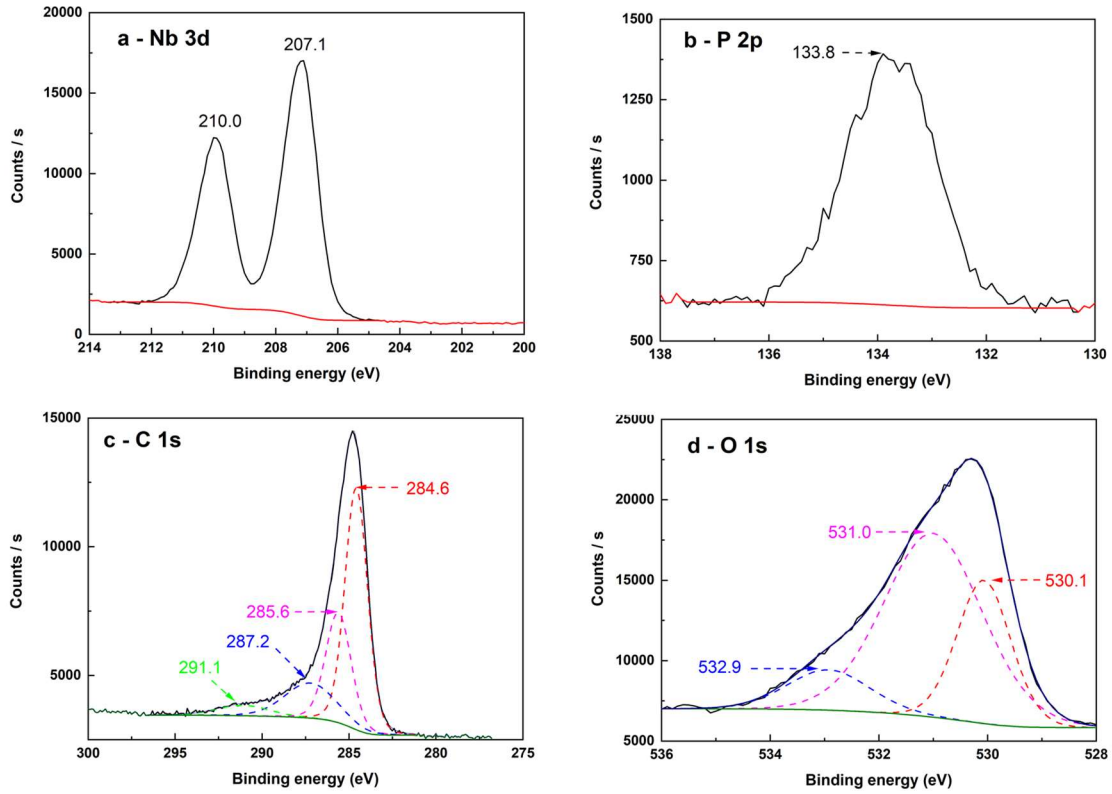

Figure 4. XPS spectra of NbP@C-RB15: (A) Nb 3d; (B) P 2p; (C) C 1s and (D) O 1s . The dashed-dotted lines represent the different component peaks obtained after deconvolution of the C 1s and O 1s XPS spectra (red for O 1s-I and C 1s-I, pink for O 1s-II and C 1s-II, blue for O 1s-III and C 1s-III and green red for C 1s-IV), while the solid navy lines are the simulated spectral envelopes.

Table 3. Binding energies of C 1s, O1s, Nb3d, P2p photopeaks and surface compositions of the different NbP@C-RB*x* catalysts

		NbP@C-RB15		**NbP@C-RB30**		**NbP@C-RB60**		**NbP@C-RB90**		**NbP@C-RB120**		**NbP@C-RB150**	
Region	**Peak**	**BE (eV)**	***Relative content %***	**BE (eV)**	***Relative content %***	**BE (eV)**	***Relative content %***	**BE (eV)**	***Relative content %***	**BE (eV)**	***Relative content %***	**BE (eV)**	***Relative content %***
Nb 3d $_{5/2}$	I	207.1	*100*	207.3	*100*	207.3	*100*	207.3	*100*	207.0	*100*	207.2	*100*
P2 2p	I	133.8	*100*	133.9	*100*	133.9	*100*	134.0	*100*	133.7	*100*	134.0	*100*
C 1s	I	284.6	*51.53*	284.8	*49.98*	284.8	*50.81*	284.8	*50.69*	284.6	*50.80*	284.9	*47.46*
	II	285.6	*26.52*	285.8	*31.91*	285.8	*28.17*	285.8	*26.58*	285.6	*24.2*	286.0	*25.30*
	III	287.2	*16.89*	287.6	*13.60*	287.5	*15.76*	287.4	*16.85*	287.0	*19.32*	287.5	*21.09*
	IV	291.1	*5.07*	291.2	*4.51*	291.0	*5.26*	291.0	*5.88*	290.7	*5.69*	291.3	*6.15*
O 1s	I	530.1	*26.38*	530.2	*34.03*	530.1	*23.95*	530.1	*16.86*	529.9	*21.96*	530.0	*14.88*
	II	531.0	*62.28*	531.2	*52.80*	531.1	*9.99*	531.1	*39.65*	531.0	*48.90*	531.0	*54.99*
	III	532.9	*11.34*	533.0	*13.16*	532.9	*26.05*	533.0	*43.50*	532.9	*29.15*	532.9	*30.13*
XPS surface composition													
Nb (surf. at. %)		6.90		6.30		3.60		3.90		3.64		4.20	
P (surf. at. %)		1.92		1.60		1.20		2.00		1.05		1.40	
N (surf. at. %)		6.38		6.60		7.10		6.30		6.89		7.36	
C (surf. at. %)		59.13		60.90		69.80		62.80		69.38		66.21	
O (surf. at. %)		25.67		24.70		18.30		25.00		19.03		20.83	
$(Nb/C)_{surf.}$		0.117		0.103		0.052		0.062		0.052		0.063	
$(Nb/O)_{surf.}$		0.268		0.255		0.197		0.156		0.190		0.202	
$(O/C)_{surf.}$		0.435		0.406		0.262		0.398		0.274		0.315	
$(P/C)_{surf.}$		0.032		0.026		0.017		0.032		0.016		0.021	
$(P/Nb)_{surf.}$		0.278		0.253		0.333		0.513		0.288		0.333	

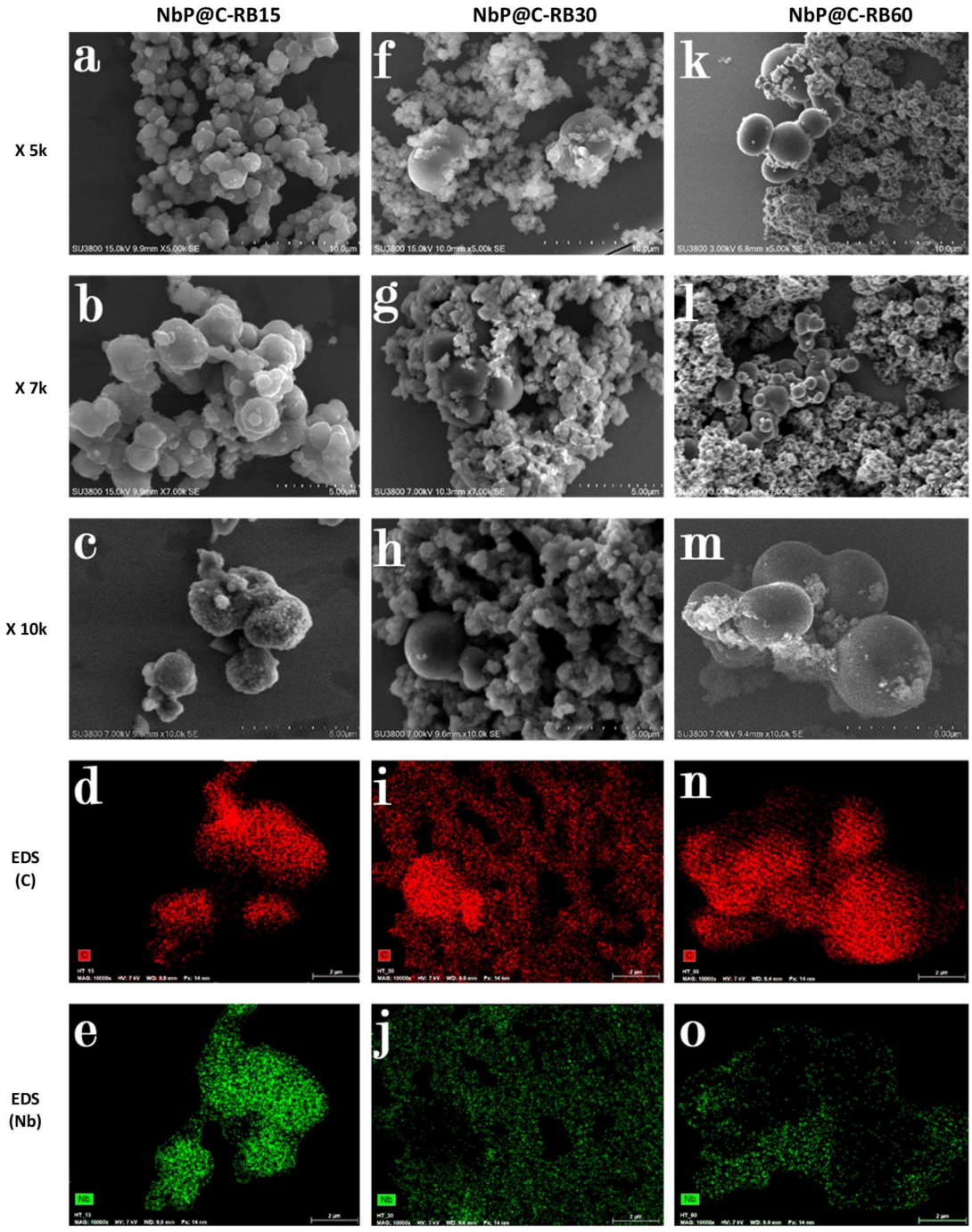

Figure 5. Representative SEM micrographs for NbP@C-RB*x* catalyst prepared with various contents of water at different magnitudes (×5k, ×7k and ×10k) for the following samples: NbP@C-RB15 (a-e), NbP@C-RB30 (f-j) and NbP@C-RB60 (k-o). Elemental analysis mapping showing the corresponding distribution of carbon (d,i,n) and niobium (e,j,o) for the micrographs taken at the highest magnification.

3.2.5. SEM-EDS analysis of catalysts

Further, SEM measurements have been carried out to investigate the morphological properties of the carbon-loaded oxide composites after H_3PO_4 treatment. For this purpose, three samples have been selected as most suitable, i.e. NbP@C-RB15, -RB30 and -RB-60. From the representative SEM images (Figure 5), we observe that spherical interconnected particles can be obtained, with a smooth and crack-free surface, and sometimes forming a peanut-like shape (Figure 5-m). In a general way, their distribution turns out to be not regular and monodisperse, and this trend is particularly evident for the HTC catalysts produced with increasing water volumes. Thus, the NbP@C-RB15 prepared from RaMe-β-CD at high concentration overall presents a better homogeneity in size of the spherical particles. It can be noticed that, for NbP@C-RB15, most of the HTC particles range in size from 1-3 μm. However, some local aggregations with densely packed spherical particles are detected on the SEM images (Figures 6-a to 6-c), which are probably the cause of the decline of porosity (surface area, pore volume and pore diameter). The distribution of the niobium and carbon species has also been investigated by SEM-EDS analysis. Figures 5-d and 5-e show representative micrographs for NbP@C-RB15. A homogeneous Nb and C distribution is visually apparent on the spherical structure, both elements appear at the same location, suggesting intimate contact.

It is revealed that changes in the morphological structure progressively appear when the NbP@C-RB*x* catalysts are prepared by using higher H_2O volumes. Thus, for NbP@C-RB30, the presence of the weakly organized granular structure, composed from particles of small sizes, still predominates (Figures 6-f to 6-h), along with some extra spherical particles of larger size (between 3 and 8 μm). As evidenced in the SEM-EDS mapping images (Figures 6-i and 6-j), niobium oxide species, together carbon species, seem to be homogeneously distributed throughout the finer grain structure. In contrast, the larger microspheres are mostly composed of carbon, being completely free from niobium. Note that the trend of forming large spherical

particles with a smooth surface is even more visible in the case of NbP@C-RB60 (Figures 6-l to 6-m). These observations suggest that large volumes of water for solubilizing the HTC reactants tends to result in a less uniform distribution of Nb species, as previously evidenced by our XPS studies. The enhanced local formation of pure carbon microspheres (bonded or not by forming peanut-like structures) can be a source of heterogeneity, which can hinder the interaction with oxide niobium species and expose more hydrophobic surfaces.

3.3. Effect of the volume of water: catalytic results

3.3.1. Series of NbP@C-RBx catalysts

The results obtained in the catalytic transformation of glucose to HMF for each the six NbP@C-RB*x* samples investigated are summarized in Figure 7, using the reaction conditions previously established.

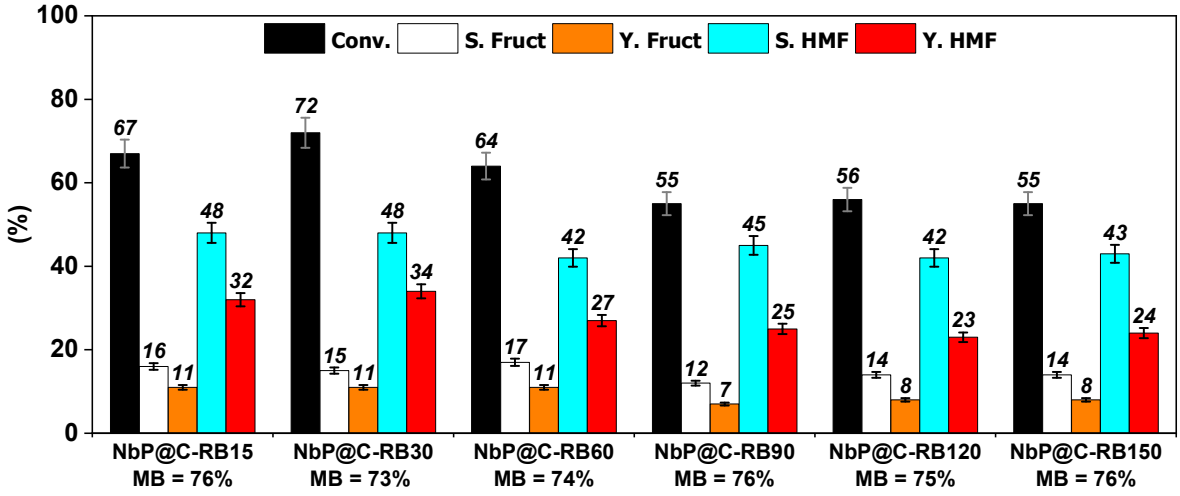

Figure 6. Aqueous phase conversion of glucose over NbP@C-CD*x* materials prepared by HTC with various H_2O volumes, and corresponding selectivity, yield for fructose and HMF and mass balance. The value in percentage of mass balance (MB) is indicated below the name of the sample. *Reaction conditions*: *Glucose concentration (3.33 wt. %); Catalyst mass: 0.2 g; Solvent: 3 mL H_2O (NaCl 33 %) and 9 mL MIBK (as extracting solvent); Reaction temperature: 150°C; Reaction time: 3 h. Pressure: 20 bar Ar.*

As shown in Figure 6, two main domains can be distinguished. Above 90 mL of water, the phosphated niobium-carbon samples all show similar behavior. Moderate conversions of glucose (55-56 %) to HMF are achieved at 150°C for 3 h, with almost constant HMF yields ranging between 23 and 25 %. These conversions are lower to those achieved under the same reaction conditions in the presence of the NbP@C-CD60, irrespective of the carbon source. When the volume of water used for the catalyst preparation is below 90 mL (or in other words, the concentration of RaMe-β-CD higher than 50 mM), a rise in conversion of at least 10 % is obtained without, however, lowering the selectivity to HMF and mass balance. Among the catalysts investigated, NbP@C-RB30 seems to exhibit the highest dehydration activity. This sample displays the highest selectivity and yield to HMF (48 % and 34 %, respectively) for the highest glucose conversion (72 %). Note also that, NbP@C-RB15 gives a similar catalytic performance, with only a small drop in conversion (- 4 % at 150°C after 3 h). It is worth noting that the results of glucose dehydration activity do not correlate with the specific surface area of the NbP@C-RB*x* catalysts. This can be readily seen by comparing the reaction rate per unit of surface area, i.e. the amount of HMF formed per unit of surface area measured after 1 h of reaction (Table 2). Thus, NbP@C-RB15, which exhibits the lowest specific surface area gives rise to the highest reaction rate, differing by more than a factor of 2.3 with NbP@C-RB30 (16.1 μmol h^{-1} m^{-2} vs 6.78 μmol h^{-1} m^{-2}).

3.3.2. Reaction monitoring as a function of time

The product distribution as function of time in the dehydration of glucose on the NbP@C-RB30 catalyst is shown in Figure 8. The results are found to be consistent with a bifunctional mechanism where the transformation of glucose proceeds first *via* the isomerization of fructose as an intermediate on Lewis acid sites followed by the dehydration on Brönsted acid sites to give HMF. Indeed, we observe that glucose is readily converted to a fairly large extent during

the first hours of reaction, achieving a conversion of 72 % for 3 h, and then remains practically constant. According to the literature [68], the formation of fructose occurs in a first stage followed by its dehydration to HMF, which happens almost instantaneously under our applied reaction conditions. Indeed, HMF becomes the major product after only 0.5 h of reaction time. Beyond this time, it is found also that the production of fructose is generated in a constant moderate yield (10-11 %), which suggests an equilibrium reaction. The results show that 3 h is the optimum reaction period to achieve the high degree of HMF product (34-35 %). Indeed, the highest selectivity to HMF is not achieved at the longer reaction time (44 % for 5 h) but at an intermediate one (48 % for 3 h), probably caused by the existence of HMF-consuming side reactions. The mass balance is also a good indicator of the occurrence of loss of matter by the formation of by-products, such as humins.

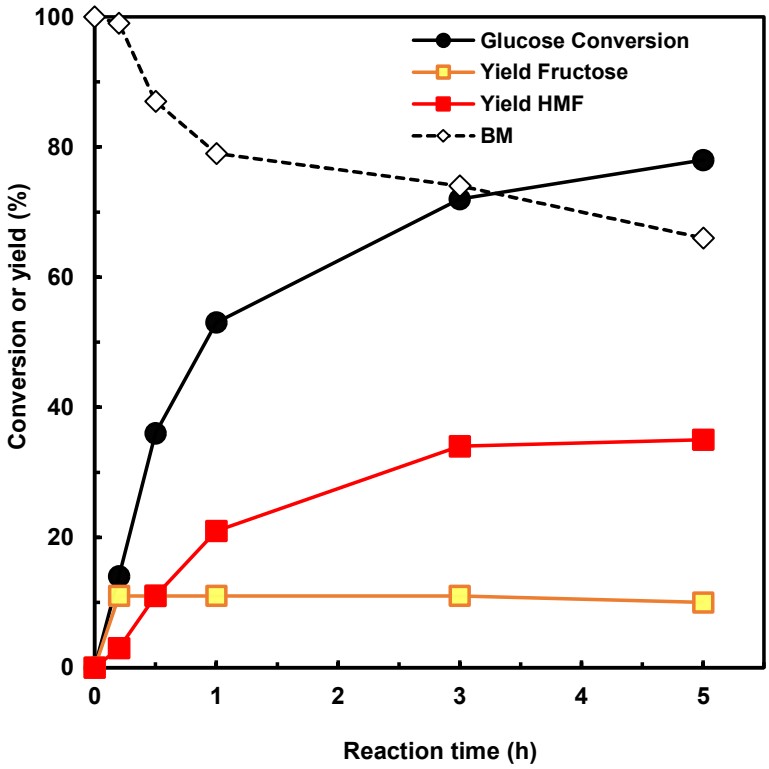

Figure 7. Product distribution obtained as a function of time from dehydration of glucose under aqueous biphasic conditions at 150°C on NbP@C-RB30 composite. *Reaction conditions*: *Glucose concentration (3.33 wt. %); Catalyst mass: 0.2 g; Solvent: 3 mL H_2O (NaCl 33 %) and 9 mL MIBK (as extracting solvent); Reaction temperature: 150°C; Pressure: 20 bar Ar.*

Our results, together with this distribution profile over NbP@C-RB30, seem to indicate a lack of Brönsted acidity, which is necessary to catalyze the dehydration reaction. In order to support this hypothesis, an additional set of catalytic experiments have been performed by adding microdoses of HCl (37 wt. %) into the reaction mixture, while all the other parameters are kept constant. It can be remembered that niobium-based solids have been initially selected for their high Lewis and Brönsted acidity on surface and their water-tolerant Lewis acid properties [15]. The HCl doses are added just before the beginning of the reaction, and the duration of each test is 0.2 h (Figure 9). The results obtained in this set of experiments provide evidence of the superior performance of NbP@C-RB30 for the direct transformation of glucose to HMF in the presence of additional HCl. This is particularly evident in the case of the test performed with 40 µL of HCl, for which the glucose conversion is more than doubled (39 vs 15 %) and the HMF yield is multiplied by about 7 (22 vs 3%). These results support the conclusions of the reaction monitoring as a function of time, confirming that the weak point of these NbP@C-CD*x* formulations is the lack of Brönsted acidity. However, if the number of Brönsted acid sites is too high, the extent of the degradation of sugars, HMF, and intermediates is inevitably enhanced.

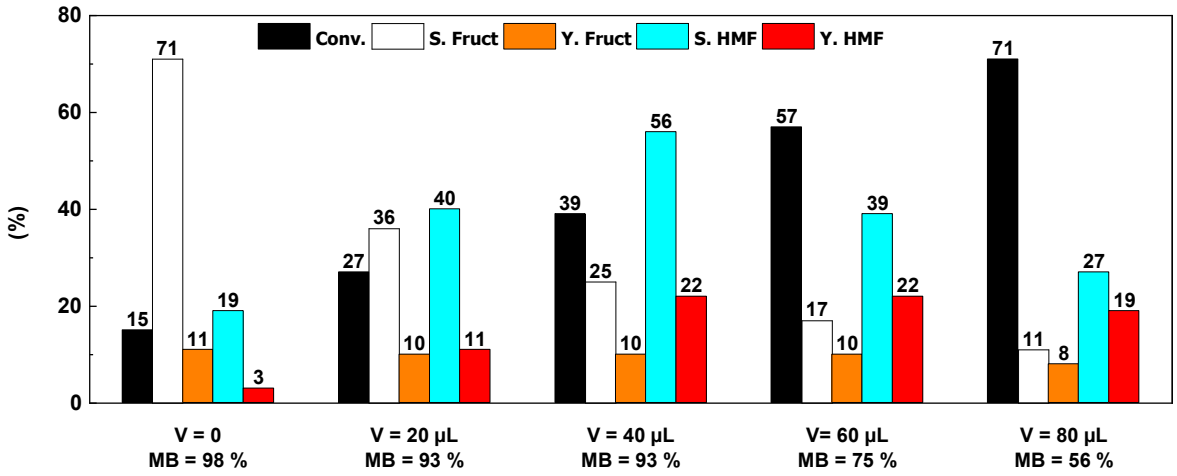

Figure 8. Influence of the addition of hydrochloric acid addition for the aqueous phase conversion of glucose in the presence of NbP@C-RB30 catalyst after 0.2 h of reaction. The

value in percentage of mass balance (MB) is indicated below the name of the sample. *Reaction conditions*: *Glucose concentration (3.33 wt. %); Catalyst mass: 0.2 g; Solvent: 3 mL H_2O (NaCl 33 %) and 9 mL MIBK (as extracting solvent); Reaction temperature: 150°C; Reaction time: 0.2 h. Pressure: 20 bar Ar.*

4. Discussion

The above characterization results have demonstrated the ability of cyclodextrins to be used as carbon sources to prepare Nb-P@C functional composites by HTC followed by a calcination step and phosphatation with H_3PO_4. However, when the HTC was performed by varying the type of CD in a fixed volume of water (60 mL), the variations were found to be minor, with a slight increase only in selectivity and yield in HMF observed with the sample prepared from RaMe-β-CD. In contrast, the morphology and structure characteristics of the NbP@C-RB*x* catalysts were shown to be much more sensitive to the volume of water used (in other words to the RaMe-β-CD concentration) during the HTC step, which in turn significantly affect the glucose dehydration catalytic properties. Thus, the best results were obtained with the NbP@C catalysts prepared with low volumes of water, i.e. NbPC@C-RB30 and more particularly NbPC@C-RB15. These conditions help to achieve a higher Nb metal dispersion in the carbon-based granular matrix, while minimizing the growth of carbon spherical particles on which the deposition of Nb oxides does not take place. It was also revealed by SEM-EDS analysis that a higher RaMeβ-CD concentration used during the HTC process (315 mM for NbP@C-RB15) was favorable for obtaining a more homogeneous and narrower size distribution of particles in a grain-like surface morphology. However, the discrepancies that have been identified between the different NbP@C-RB*x* samples by XPS and SEM-EDS may not be the only explanation for the above results. Besides, in aqueous biphasic catalysis with liquid-liquid interfacial areas, the surface wettability of the heterogeneous catalyst is also known to play a prominent role in regulating the interaction between the reactants and the surface. In the case of composite

materials, the dispersibility, which is closely dependent on the surface properties, can be complex, potentially with both hydrophilic and hydrophobic regions. Indeed, the surface covered with amorphous Nb_2O_5 and acidic surface OH groups are generally assumed to be hydrophilic [69]. In contrast, graphitic carbons should be rather considered as lightweight and hydrophobic materials.. Interestingly, we have found that the dispersibility of the NbP@C-RB*x* samples differed according to the volume of water used during the HTC preparation. Figure 10 displays the photographs of the biphasic organic (MIBK) /aqueous system in the presence of NbP@C-RB*x* (with x = 15, 30 and 60). Evidence for the affinity of NbP@C-RB15 towards the water is readily demonstrated in Figure 9-a. The latter, in fact, is entirely located in the water phase (lower phase), confirming its hydrophilicity. By preparing the catalyst in 30 mL of water, the picture shows that NbP@C-RB30 tends to partition in the aqueous phase and at the water-MIBK interface (Figure 9-b), suggesting the occurrence of some hydrophobicity. This increase in hydrophobicity is even more visible with NbP@C-RB60 interface (Figure 9-c), which remains preferentially dispersed in the organic phase (upper phase) and at the interfacial region.

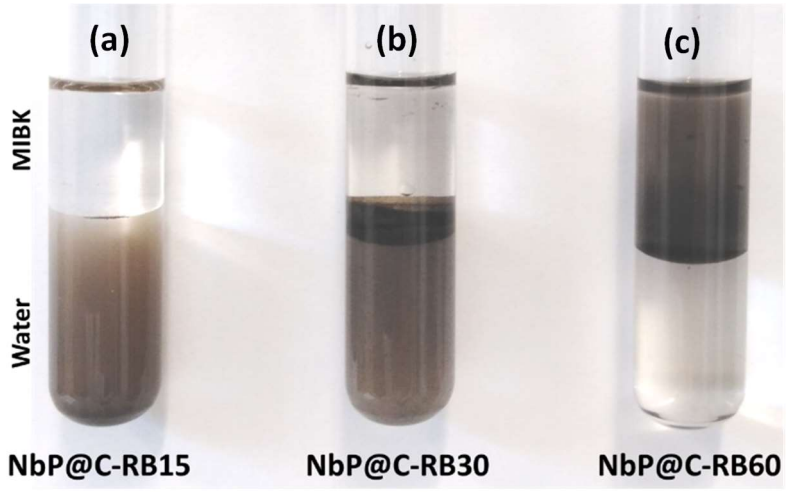

Figure 9. Photographs displaying the distribution of the NbPC@RB*x* samples [x = 15 (a), 30 (b) and 60 (c)] in a mixture of water-MIBK. *Experimental conditions: 10 mg of catalyst; 3 mL of MIBK; 3 mL of water. The mixture was treated under ultrasound for 5 minutes at room temperature and left to stand under static conditions until complete decantation.*

These observed changes can be explained by assuming that variations in water volumes during the HTC process affect the hydrophobic/hydrophilic nature of the NbP@C composite surfaces and their partition behavior in the biphasic system. Thus, despite the low specific surface area of NbP@C-RB15, this sample not only shows the highest density of surface Nb species (Nb/C= 0.117 vs Nb/C = 0.052 for NbP@C-RB60), but also the best surface dispersibility in water. The positioning of this catalyst in water seems to be the most appropriate for ensuring the contacts with glucose and intermediate fructose (both being water-soluble) and consequently leading to an increase in efficiency of the overall conversion of glucose to HMF.

5. Conclusion

In summary, we have shown that phosphated niobium oxide-carbon composites could be obtained through HTC by using cyclodextrins as original carbon sources in the presence of ammonium niobium oxalate. After calcination and H_3PO_4 phosphatation, the resulting catalysts were evaluated in the direct conversion of glucose to 5-hydroxymethylfurfural. Several types of cyclodextrins were examined for the HTC process with identical volumes of water (60 mL), without showing any significant differences between them. In a further optimization, where the randomly methylated β-CD was selected for its higher solubility and its substantial surface activity, we observed that the adjustment of the concentration affected in a more substantial way the surface dispersion of the niobium oxide species anchored on the carbon-based nanostructures and the morphological structures of the resulting composites, but also their dispersion and partitioning in aqueous biphasic systems. NH_3-TPD monitored by mass spectroscopy revealed that the materials have predominantly the same strength of Lewis and Brönsted acidity with moderate strengths. Among the different catalysts investigated, those prepared from the higher concentrations of RaMe-β-CD (or to the lower water volumes) where

surface Nb(V)oxide species are linked to the carbon frameworks affords an increase of the niobium surface sites. Despite the low specific surface area of NbP@C-RB15 (33 m^2/g), a high HMF yield of 32 % and a glucose conversion of 67 % were achieved within 3 h at a glucose concentration of 3.33 wt. % in water-NaCl/MIBK biphasic conditions (150°C, 3h). Notably, this catalyst exhibits a comparable activity to most reported niobium-based catalysts tested under similar aqueous biphasic conditions [21,31-33]. This effect was mainly attributed to both an increase in the density of surface Nb active species and a suitable positioning of the catalyst in the water phase of the biphasic solvent system with MIBK, promoting the chemical reactions of glucose dehydration to occur.

Acknowledgments

Walid Hamza Saadaoui is grateful to the IFMAS (Institut Français des Matériaux Agro-Sourcés) and Roquettes Frères (Lestrem) for the funding of his PhD grant. The authors acknowledge the Chevreul Institute (FR 2638), Ministère de L'Enseignement Supérieur et de la Recherche, Région Nord-Pas de Calais and FEDER program for supporting and partially funding this work. The authors thank Laurence Burylo, Olivier Gardoll and Martine Trentesaux (University of Lille for their respective assistance in XRD, NH_3-TPD and XPS analyses. The authors are also grateful to Dr. Antonio Da Costa (UCCS, University of Artois) for the SEM-EDS measurements.

CRediT authorship contribution statement

Walid Hamza Saadaoui: Investigation, Visualization, Writing - Original Draft. **Cécile Machut:** Methodology, Investigation, Validation **Sébastien Rio**: Investigation, Validation. **Sandra Bigot**: Validation, Resources. **Vincent Wiatz:** Conceptualization, Resources. **Eric Monflier:** Conceptualization, Writing - Review & Editing. **Anne Ponchel**: Project administration, Methodology, Investigation, Supervision; Writing - Review & Editing.

References

[1] E. Dahlquist, in : Biomass as Energy Source: Resources, Systems and Applications, 1st edition, CRC Press, London, 2012.

[2] F. Cherubini, Energy Convers. Manage. 51 (2010) 1412-1421.

[3] C. Rosenfeld, J. Konnerth, W. Sailer-Kronlachner, P. Solt, T. Rosenau, H. W. G. van Herwijnen, ChemSusChem 13 (2020) 3544-3564.

[4] F. Menegazzo, E. Ghedini, M. Signoretto, Molecules 23 (2018) 2201.

[5] J.J. Bozell, G. R. Petersen, Green Chem. 12 (2010) 539-554.

[6] Y. W Hsiao, A. Anastasopoulou, M. Ierapetritou, D. G. Vlachos, Green Chem.23 (2021) 4008-4023.

[7] Y. Roman-Leshkov, J. A. Dumesic, Top. Catal. 52 (2009) 297-303.

[8] Y. Roman-Leshkov, J. N. Chheda, J. A. Dumesic, Science 312 (2006) 1933-1937.

[9] A. Al Ghatta, J. D. E. T. Wilton-Ely, J. P. Hallett, Green Chem. 23 (2021) 1716-1733

[10] E. C. Sindermann, A. Holbach, A. de Haan, N. Kockmann, Chem. Eng. J. 283 (2016) 251-259.

[11] L. F. Zhu, X. Fu, Y. X. Hu, C. W. Hu, ChemSusChem, 13 (2020) 4812-4832.

[12] L. Shuai, J. S. Luterbacher, ChemSusChem 9 (2016) 133-155.

[13] K. V. Wagh, K. C. Badgujar, N. M. Patil, B. M. Bhanage, Curr. Org. Chem. 20 (2016) 736-751.

[14] P. Carniti, A. Gervasini, S. Biella, A.Auroux, Chem. Mater. 15 (2005) 6128-6136.

[15] K. Tanabe, Mater. Chem. Phys. 17 (1987) 217-225.

[16] K. Nakajima, Y. Baba, R. Noma, M. Kitano, J. N. Kondo, S. Hayashi, M. Hara, J. Am. Chem. Soc. 133 (2011) 4224-4227.

[17] B. Guo, L.Ye, G. Tang, L. Zhang, B. Yue, S. C. E. Tsang, H. He, Chin. J. Chem. 35 (2017) 1529-1539.

[18] H. T. Kreissl, K. Nakagawa, Y.-K. Peng, Y. Koito, J. Zheng, S. C. E. Tsang, J. Catal 338 (2016) 329-339

[19] F. Huang, T. Jiang, H. Dai, X. Xu, S. Jiang, L. Chen, Z. Fei, P. J. Dyson, Catal. Lett. 150 (2020) 2599-2606.

[20] C. Carlini, M. Giuttari, A. M. Raspolli Galletti, G. Sbrana, T. Armaroli, G. Busca, Appl. Catal., A 183 (1999) 295-302.

[21] Y. Zhang, J. Wang, X. Li, X. Liu, Y. Xia, B. Hu, G. Lu, Y. Wang, Fuel 139 (2015) 301-307.

[22] P. Carniti, A. Gervasini, F. Bossola, V. Dal Santo, Appl. Catal., B 193 (2016) 93-102.

[23] M. N. Catrinck, E. S. Ribeiro, R. S. Monteiro, R. M. Ribas, M. H. P. Barbosa, R. F. Teófilo, Fuel 210 (2017) 67-74.

[24] S. Souzanchi, L. Nazari, K. T. V. Rao, Z. Yuan, Z. Tan, C. C Xu, J. Ind. Eng. Chem. 101 (2021) 214-226.

[25] J. L. Vieira, G. Paul, G. D. Iga, N. M. Cabral, J. M. C. Bueno, C. Bisio, J. M. R. Gallo, Appl Catal., A 617 (2021) 118099.

[26] V. V. Ordomsky, V. L. Sushkevich, J. C. Schouten, J. Van Der Schaaf, T. A. Nijhuis, J. Catal. 300 (2013) 37-46.

[27] B. Torres-Olea, C García-Sancho, J. A. Cecilia, M. Oregui-Bengoechea, P. L. Arias, R. Moreno-Tost, P. Maireles-Torres, Mol. Catal. 510 (2021) 111685.

[28] M. T. Reche, A. Osatiashtiani, L. J. Durndell, M. A. Isaacs, A. Silva, A. F. Lee, K. Wilson, Catal. Sci. Technol. 6 (2016) 7334-7341

[29] N. Candu, M. El Fergani, M. Verziu, B. Cojocaru, B. Jurca, N. Apostol, C. Teodoresu, V. I. Parvulescu, S. M. Coman, Catal. Today 325 (2019) 109-116.

[30] A. Tirsoaga, V. Kuncser, V. I. Parvulescu, S. M. Coman, Catalysis Today 366 (2021) 48-56.

[31] H. Xiong, T. Wang, B. H. Shanks, A. K. Datye, Catal. Letters 143 (2013) 509-516.

[32] X. Li, K. Peng, Q. Xia, X. Liu, Y. Wang, Chem. Eng. J. 332 (2018) 528-536.

[33] M. El Fergani, N. Candu, M. Tudorache, C. Bucur, N. Djelal, P. Granger, S. M. Coman Appl. Catal., A 618 (2021) 118130.

[34] H. N. Phama, Y. J. Pagan-Torres, J. C. Serrano-Ruiz, D. Wang, J. A. Dumesic, A. K. Datye, Appl. Catal., A 397 (2011) 153-162.

[35] Y. J. Pagan-Torres, J. M. R. Gallo, D. Wang, H. N. Pham, J. A. Libera, C. L. Marshall, J. W. Elam, A. K. Datye, J. A. Dumesic, ACS Catal. 1 (2011) 1234-1245.

[36] H. Xiong, H. N. Pham, A.K. Datye, J. Catal. 302 (2013) 93-100.

[37] A. Biwer, G. Antranikian, E. Heinzle, Appl. Microbiol. Biotechnol. 59 (2002) 609-617.

[38] A. Nadia Morin-Crini, S. Fourmentin, E. Fenyvesi, E. Lichtfouse, G. Torri, M. Fourmentin, G. Crini, Env. Chem. Lett. 19 (2021) 2581-2617.

[39] E. Norkus, J. Incl. Phenom. Macrocycl. Chem. 65 (2009) 237-248.

[40] D. Prochowicz, A. Kornowicz, I. Justyniak, J. Lewinski, Coord. Chem. Rev. 306 (2016) 331-345.

[41] S. D. Eastburn, B. Y.Tao, Biotechnology Adv. 12 (1994) 325-339.

[42] B. H. Han, W. Zhou, A. Sayari, J. Am. Chem. Soc. 125 (2003) 3444-3445.

[43] W. Shen, X. Yang, Q. Guo, Y. Liu, Y. Song, Z. Han, Q. Sun, J. Cheng, Mater. Lett. 60 (2006) 3517-3521.

[44] Y. Shin, L.-Q. Wang, I.-T. Bae, B. W. Arey, G. J. Exarhos, J. Phys. Chem. C 112 (2008) 14236-14240.

[45] H. C. Wang, B. L. Li, J. T. Li, P. Lin, X. B. Bian, J. Li, B. Zhang, Z. X. Wan, Appl. Surf. Sci. 257 (2011) 4325-4330.

[46] J. E. St. Dennis, P. Venkataraman, J. He, V. T. John, S. J. Obrey , R. P. Currier, M. Lebrón-Colón, F. J. Sola, M. A. Meador, Carbon 49 (2011) 718-722.

[47] Z.-C. Yang, Y. Zhang, J.-H. Kong, S. Y. Wong, X. Li, J. Wang, Chem. Mater. 25 (2013) 704-710.

[48] M. Zanetti, A. Anceschi, G. Magnacca, G. Spezzati, F. Caldera, G. P. Rosi, F. Trotta, Microporous Mesoporous Mater. 235 (2016) 178-184.

[49] S.-C. Shen, S.-L. Xu, S. Zhao, L.-L. Zhang, S-Q. Chu, H.-W. Liang, ACS Sustainable Chem. Eng. 10 (2022) 731-737.

[50] S. Sadjadi, F. Koohestani, B. Léger, E. Monflier, Appl Organometal Chem. 33 (2019) e5213.

[51] N. Gokulakrishnan, G. Peru, S. Rio, J.-F. Blach, B. Léger, D. Grosso, E. Monflier, A. Ponchel, J. Mater. Chem. A 5 (2014) 6641–6648.

[52] S. Rio, G. Peru, B. Léger, F. Kerdi, M. Besson, C. Pinel, E. Monflier, A Ponchel, J. Catal. 383 (2020) 343-356.

[53] S. A. Nicolae, H. Au, P. M. Modugno, H. Luo, A. E. Szego, M. Qiao, L. Li, W. Yin, H. J. Heeres, N. Berge, M.-M. Titirici, Green Chem. 22 (2020) 4747-4800.

[54] L. Bahcivanji, G. Gascó, J. Paz-Ferreiro, A. Méndez, Waste Manage. 106 (2020) 55-61

[55] S. Okazaki, M. Kurimata, T. Iizuka, K. Tanabe, Bull. Chem. Soc. Jpn. 60 (1987) 37-41

[56] L. Leclercq, H. Bricout, S. Tilloy, E. Monflier, J. Colloid Interface Sci. 307 (2007) 481-487.

[57] H. P. Boehm, Carbon 32 (1994) 759-769.

[58] S. Li, Q. Xu, E. Uchaker, X. Cao, G. Cao, CrystEngComm 18 (2016) 2532-2540.

[59] I. Jiménez-Morales, M. Moreno-Recio, J. Santamaría-González, P. Maireles-Torres, A. Jiénez-López, Appl. Catal., B 164 (2015) 70-76.

[60] Q. Xu, Z. Zhu, Y. Tian, J. Deng, J. Shi, Y. Fu, Bioresources 9 (2014), 303-315.

[61] M. Nahavandi, T. Kasanneni, Z. S. Yuan, C. C. Xu, S. Rohani, ACS Sustainable Chem. Eng. 7 (2019) 11970-11984.

[62] T. Cserhati, J. Szejtli, Tenside Detergents 22 (1985) 237-238

[63] M. Sevilla, A. B. Fuertes, Chem. Eur. J. 15 (2009) 4195-4203.

[64] P. H. F. Pereira, H. J. C. Voorwald, M. O. H. Cioffi, M. L. C. P. Da Silva, A. M. B. Rego, A. M. Ferraria, M. N. De Pinho, Cellulose 21 (2014) 641-652.

[65] Y. Wang, S. Zuo,J . Yang, S.-H. Yoon, Langmuir 33 (2017) 3112-3122.

[66] L. F. Sharanda, Y. V. Plyuto, I. V. Babich, I. V. Plyuto, A. P. Shpak, J. Stoch, J. A. Moulijn, Appl. Surface Sci. 252 (2006) 8549-8556.

[67] C. García-Sancho, J. M. Rubio-Caballero, J. M. Mérida-Robles, R. Moreno-Tost, J. Santamaría-González, P. Maireles-Torres, Catal. Today 234 (2014) 119-124.

[68] H. E. van Dam, A. P. G. Kieboom, H. van Bekkum, Starch/Stärke, 38 (1986) 95-101.

[69] M. Tanaka, H. Shima, T. Yokoi, T. Tatsumi, J.N. Kondo. Catal Lett 141 (2011) 283-292.